NMR IN BIOMEDICINE
NMR Biomed. 1999;**12**:51–62

Multi-component apparent diffusion coefficients in human brain†

Robert V. Mulkern,[1]* Hakon Gudbjartsson,[2] Carl-Fredrik Westin,[2] Hale Pinar Zengingonul,[2] Werner Gartner,[3] Charles R. G. Guttmann,[2] Richard L. Robertson,[1] Walid Kyriakos,[1] Richard Schwartz,[2] David Holtzman,[4] Ferenc A. Jolesz[2] and Stephan E. Maier[2]

[1]Department of Radiology, Children's Hospital, Harvard Medical School, Boston, MA 02115, USA
[2]Department of Radiology, Brigham and Women's Hospital, Harvard Medical School, Boston, MA, USA
[3]Department of Biotechnology, University of Technology, Graz, Austria
[4]Department of Neurology, Massachussetts General Hospital, Harvard Medical School, Boston, MA, USA

Received 14 January 1998; revised 30 March 1998; accepted 2 April 1998

ABSTRACT: The signal decay with increasing *b*-factor at fixed echo time from brain tissue *in vivo* has been measured using a line scan Stejskal–Tanner spin echo diffusion approach in eight healthy adult volunteers. The use of a 175 ms echo time and maximum gradient strengths of 10 mT/m allowed 64 *b*-factors to be sampled, ranging from 5 to 6000 s/mm^2, a maximum some three times larger than that typically used for diffusion imaging. The signal decay with *b*-factor over this extended range showed a decidedly non-exponential behavior well-suited to biexponential modeling. Statistical analyses of the fitted biexponential parameters from over 125 brain voxels ($15 \times 15 \times 1$ mm^3 volume) per volunteer yielded a mean volume fraction of 0.74 which decayed with a typical apparent diffusion coefficient around 1.4 μm^2/ms. The remaining fraction had an apparent diffusion coefficient of approximately 0.25 μm^2/ms. Simple models which might explain the non-exponential behavior, such as intra- and extracellular water compartmentation with slow exchange, appear inadequate for a complete description. For typical diffusion imaging with *b*-factors below 2000 s/mm^2, the standard model of monoexponential signal decay with *b*-factor, apparent diffusion coefficient values around 0.7 μm^2/ms, and a sensitivity to diffusion gradient direction may appear appropriate. Over a more extended but readily accessible *b*-factor range, however, the complexity of brain signal decay with *b*-factor increases, offering a greater parametrization of the water diffusion process for tissue characterization. Copyright © 1999 John Wiley & Sons, Ltd.

KEYWORDS: brain; apparent diffusion coefficient (ADC); biexponential *b*-factor decay

INTRODUCTION

Diffusion imaging for neuroradiologic evaluation of stroke has attained significant clinical relevance.[1–10] The ability to explore anisotropic diffusion of water due to fiber orientation in brain or muscle[11–15] has also driven the development and application of diffusion imaging techniques. Several microscopic models of how water molecules move within tissue have been forwarded to describe research and clinical findings in diffusion imaging. For instance, the separation of perfusive motions in the microvasculature from "Brownian" motion within the non-vascular extra- and intracellular water compartments has been proposed based on the difference in their relative apparent diffusion coefficient (ADC) values.[16–18] Most practitioners, however, employ a simpler model in which a single ADC of brain water dominates. The sensitivity of this ADC value to the direction of the diffusion sensitization gradient in some parts of the brain is well recognized and attributed to anisotropic diffusion along myelinated axons in the white matter. With this "standard" model, a single two-point *b*-factor measurement for six different diffusion sensitization directions suffices to yield a theoretically complete description of the full diffusion tensor for each voxel sampled.[12,13] Within the framework of the standard model, the use of multiple *b*-factor measurements along any given direction would only serve to improve the precision of the measurement while not adding to the overall information content.

In this work, using a 1.5 T imaging system with conventional gradient hardware, the validity of the 'standard' model for human brain is tested *in vivo* by making multiple *b*-factor measurements over a much larger range than that typically used for routine diffusion imaging. The study was motivated in part by recent work from Niendorf *et al.*,[19] who reported a departure from purely monoexponential signal decay in rat brain using a 4.7 T

**Correspondence to:* R. V. Mulkern, Department of Radiology, Children's Hospital, 300 Longwood Avenue, Boston, MA 02115, USA.
E-mail: mulkern@bwh.harvard.edu
†Presented in part at the 1997 meeting of the Radiological Society of North America.

CCC 0952–3480/99/010051–12 $17.50

magnet equipped with large gradient capabilities. We demonstrate that similar behavior in human brains is observable with standard 1.5 T clinical systems and report what may be classified as a second apparent diffusion component of the signal decay at large *b*-factors.

MATERIALS AND METHODS

Scanning was performed with a 1.5 T Signa scanner (General Electric Medical Systems, Milwaukee, WI) operating at the 5.4 hardware/software configuration using the standard head quadrature coil. From a set of 15 mm thick axial T_1-weighted images ($TR/TE = 500/20$), a supratentorial slice was selected at approximately the level of the putamen. A 225 mm^2 cross-sectional column extending left-to-right and passing through cortex, subcortical white matter, external capsule, putamen, internal capsule and thalamus at the level of the third ventricle was then chosen for interrogation. The location of the selected column was confirmed by imaging the selected plane with a rapid scout sequence preceded by a saturation pulse outlining the selected tissue column, as described previously.[20] Diffusion measurements of the tissue column were performed with an inner volume spin-echo sequence similar to that described by Chenevert *et al.*[21,22] Mutually orthogonal slice selective excitation and refocusing pulses were used to solicit an echo from the intersection of the two slices. Standard frequency encoding was performed for along-column spatial mapping, allowing a one-dimensional image of the column to be generated each repetition time TR. Unless otherwise specified, a receiver bandwidth of 16 kHz and 256 frequency encoding steps were used to sample the echo to obtain an along column spatial resolution of approximately 1 mm. Most studies utilized 15 mm thick slice selection pulses so that minimal voxel sizes were $15 \times 15 \times 1$ mm^3. A long echo time of 175 ms was employed to accommodate heavy diffusion weighting with long duration Stejskal–Tanner pulsed field gradients placed about the refocusing pulse.[23] Unless otherwise stated, all three gradient axes were used for diffusion sensitization in a (1,1,1) configuration. The amplitude, *G*, of the diffusion gradient was incremented every *TR* period to cover a wide range of *b*-factors from 5 to 6000 s/mm^2 in 64 equal steps. The *b*-factor was calculated through the standard relation

$$b = 3(\gamma\delta G)^2(\Delta - \delta/3) \qquad (1)$$

where δ is the duration of each diffusion gradient lobe and Δ the times between their leading edges, which in our experiments were 79.6 and 82.9 ms. In one set of experiments, the *b*-factor range was reduced to cover 5–2000 s/mm^2 by using only one gradient direction, *x*, *y* or *z*, for diffusion sensitization.

With a 4 s *TR* to minimize T_1-saturation effects, an image consisting of 64 lines, each being a magnitude one-dimensional map of the column at a different *b*-factor, was generated in 4 min 18 s. A total of eight healthy adult volunteers were studied in this manner. Three glass vials containing ethanol, isopropanol and saline, respectively, were placed in a row and scanned in the same manner as the volunteers.

Additional studies with a 3 mM $NiCl_2$ doped solution in a spherical phantom were performed to assess the influence of cross-terms from imaging gradients on diffusion measurements and to assess signal-to-noise properties. Column thicknesses of 15×15 mm^2 and 10×10 mm^2, with refocusing lobes placed immediately after the 90° pulses, were tested using slice select gradient strengths of 1.8 and 2.6 mT/m, respectively. For each slice thickness, three pairs of receiver bandwith (in kHz) and number of frequency encoding steps were tested. These were 16/256, 8/128 and 4/64, all keeping the same echo readout duration of 8 ms, but with decreasing readout and pre-readout gradient strengths of 3.13, 1.56 and 0.78 mT/m, respectively, with the pre-readout applied during the 90°–180° interval. Diffusion coefficients of water (D_{water}) were calculated from the signal decay with *b*-factor using a monoexponential function of the form:

$$S = A\exp(-bD_{water}) + B \qquad (2)$$

where *A* is the extrapolated amplitude at $b = 0$ and *B* is the positive baseline noise value in magnitude calculated data[24] as measured from a large region-of-interest outside the phantom. An experimental measure of signal-to-noise (S/N) was calculated from *A*/*B* and used to test the following proportionality relation for S/N derived from standard considerations[25] adjusted for this particular imaging mode:

$$\text{S/N} \propto (\text{FOV}) \times (\text{slice thickness})^2/[(\text{bandwidth}) \times (\text{no. of frequency encodes})]^{1/2} \qquad (3)$$

where FOV in this case is the length of the column.

To assess partial volume averaging effects, an additional study on one volunteer was performed with 10 mm thick slice selective pulses to sample a deep gray matter structure, the putamen, with minimal contributions from other structures. The tissue column was positioned using a set of 3 mm thick contiguous slices in the axial plane acquired with a T_2-weighted fast spin-echo sequence. These images allowed for the placement of the 10×10 mm^2 column in a manner which ensured minimal partial volume averaging effects for diffusion measurements from the putamen using a 0.4 ml volume.

Data analysis was performed off-line with Sun workstations using Matlab software (The Math Works Inc., Natick, MA). A non-linear least squares Marquardt algorithm was employed to fit brain signal intensity decay with *b*-factor from approximately 125 brain voxels

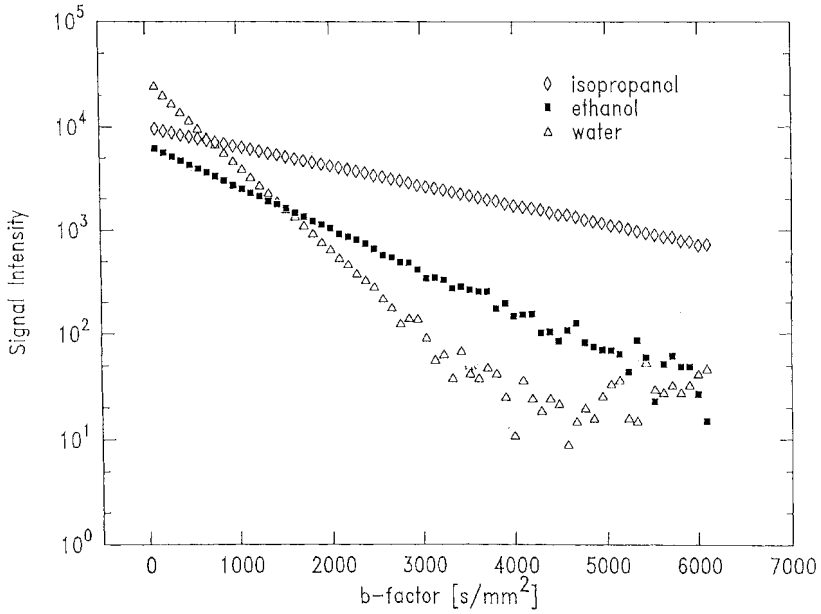

Figure 1. Signal decay with *b*-factor from three different phantoms containing isopropanol, ethanol and isotonic water. The decays are clearly monoexponential with slopes yielding diffusion coefficients in agreement with literature values[19]

per individual to a biexponential function of the form

$$S = A_1 \exp(-D_1 b) + A_2 \exp(-D_2 b) \qquad (4)$$

Here, A_1, A_2 and D_1, D_2 are the amplitudes and apparent diffusion coefficients, respectively, of the diffusion induced signal attenuation for the two components in this model. The first two *b*-factors were excluded from the analyses to avoid contamination from any "perfusion" or cerebrospinal fluid component with very high ADC values unrepresentative of pure brain tissue.[16,17] Attempts to fit brain signal decay curves with monoexponential functions over the *b*-factor range 195–6000 s/mm^2 led to χ^2 values over an order of magnitude larger than those obtained from biexponential fits. Triexponential fitting functions over this *b*-factor range yielded unstable parametrization with no significant decrease in χ^2 values compared with those obtained from biexponential fits. In contrast, for all three liquids studied, attempts to fit signal intensity vs *b*-factor with other than the monoexponential function of eq. (2) were unwarranted.

RESULTS

Figure 1 shows a semi-log plot of signal decay with increasing *b*-factor for isopropanol, ethanol and isotonic water phantoms using the same imaging gradients employed for the *in vivo* brain studies of the eight healthy adult volunteers. The lack of any noticeable curvature in these plots for signal intensities above baseline noise levels demonstrates that in simple isotropically diffusing solutions, the purely monoexponential signal decay expected is indeed observed. No curvature or departure from a straight line is observed until baseline noise values are reached, as seen particularly for the water signal at high *b*-factors due to its relatively large diffusion coefficient compared with the other substances. The diffusion coefficients obtained from the slopes of the decay curves in Fig. 1 were 0.44 μm^2/ms (isopropanol), 0.95 μm^2/ms (ethanol), and 1.95 μm^2/ms (saline), which are in good agreement with literature values.[19]

Signal decay curves extracted from the more extensive phantom testing performed with the $NiCl_2$ doped water phantom at variable imaging gradient parameters are provided in Fig. 2. Each of these decay curves achieves baseline noise values at large *b*-factors due to the high diffusion coefficient of water. Fits to the data using eq. (2), which included measured baseline noise values, are shown as solid lines in the figure. For signal values above the baseline noise, changing the slice thicknesses of the excitation and refocussing pulses from 15 to 10 mm resulted in signal decreases of approximately 64%, as predicted by eq. (3). Changing the bandwidth/no. of frequency encode steps primarily affected the baseline noise values, in a manner completely consistent with eq. (3). The mean diffusion coefficient from all six measurements was 2.02 ± 0.10 with a difference of less than 15% between the highest and lowest recorded values, indicating only minor effects on diffusion measurement from image gradient cross-term contributions to the *b*-factor unaccounted for by eq. (1). Table 1

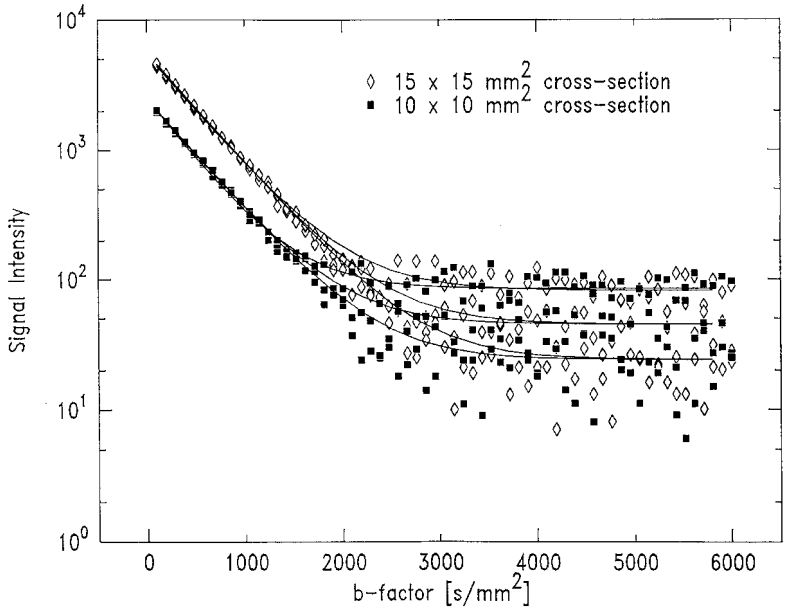

Figure 2. Signal decay with *b*-factor from a lightly doped water phantom acquired with different imaging parameters (see text for details). Diffusion coefficients and signal-to-noise properties extracted from the solid line fits using a monoexponential with baseline noise model are given in Table 1. The lack of any significant deviation in measured ADC with changes in slice select and/or read gradient amplitudes indicates the minimal influence of cross-term effects from imaging gradients to the diffusion measurement

summarizes the results from this phantom experiment and includes a comparison of experimentally measured signal-to-noise values with those predicted by eq. (3).

Table 1. Results from $NiCl_2$ phantom experiments with variable image gradient settings as obtained from diffusion analyses based on eqs (2) and (3). Sequences I–III utilized $15 \times 15\ mm^2$ tissue column cross-sections with bandwidth/no of frequency encode settings of 16/256, 8/128 and 4/64, respectively, with bandwidth reported in kHz. Sequences IV–VI utilized $10 \times 10\ mm^2$ tissue column cross-sections with bandwidth/no of frequency encode settings of 16/256, 8/128 and 4/64, respectively. The *b*-factor range as calculated from eq. (1) with only the diffusion sensitizing gradients considered was 5–6000 s/mm^2, as with the brain studies. Only minor variations in the diffusion coefficient are observed as the imaging gradient parameters vary, indicating little influence of cross-terms on diffusion measurement. The signal-to-noise ratios reported experimentally as A/B_{expt} are in good agreement with those predicted as S/N_{pred}

	A	D (μm^2/ms)	B	A/B_{expt}	S/N_{pred}
I	5297	2.00	87	61	61[a]
II	5481	1.97	45	122	122
III	5584	1.96	24	233	244
IV	2416	2.23	85	28	27
V	2396	2.00	45	53	54
VI	2453	1.97	24	102	108

[a] This was an assumed agreement with A/B_{expt} from which the remaining S/N_{pred} values were calculated using eq. (3).

There is an excellent correspondence between experimental and predicted signal-to-noise values with a linear regression analysis yielding a correlation coefficient greater than 0.99.

Figure 3(a) shows a T_1-weighted axial brain image with the left-to-right tissue column targeted for interrogation outlined by the horizontal white bars. Figure 3(b) shows this tissue column as a function of *b*-factor for values ranging from 5 to 6000 s/mm^2 in steps of approximately 95 s/mm^2. The vertical axis is ascending *b*-factor from top to bottom. Note the sustained signal with *b*-factor from lipid signal in the scalp attributed to the very low diffusion coefficient of triglycerides. Also, in the central regions of the brain corresponding to internal capsule, a sustained signal at large *b*-factors is observed. Typical plots of signal decay with increasing *b*-factor from $15 \times 15 \times 2\ mm^3$ voxels in the internal capsule, the cortex, and the scalp are shown in Fig. 4. A marked curvature on these semi-log plots for the brain tissue voxels is indicative of non-monoexponential behavior. The solid lines through the brain data are fits to the biexponential function given in eq. (4). A monoexponential fit is shown as a solid line through the signal decay from the scalp voxel, whose signal is attributed to lipids in the form of methylene and methyl protons.

Figure 5 shows results from fitting all the brain voxels in one volunteer with the biexponential function. Shown is the original data (top), and in descending order the

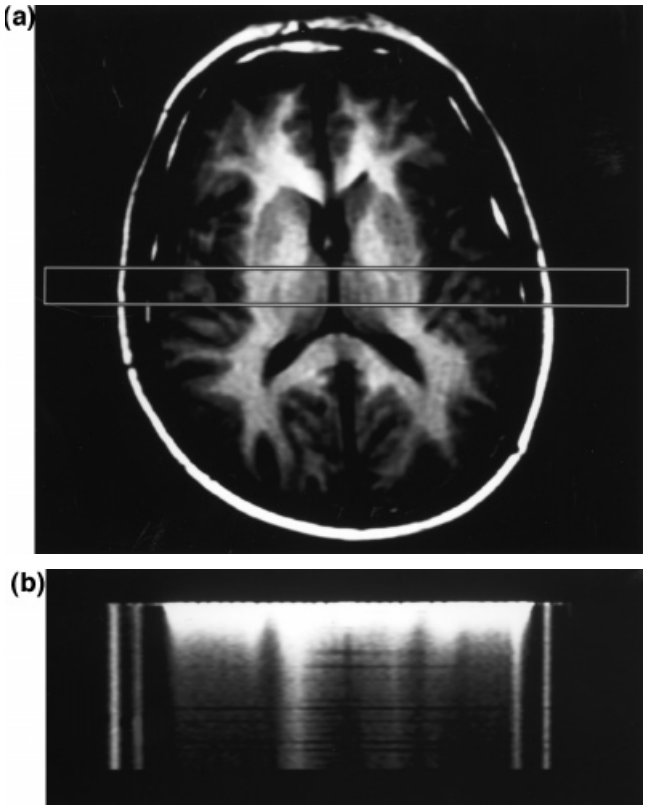

Figure 3. (a) T_1-weighted scout image showing a 15 mm thick axial slice with the tissue column targeted for interrogation outlined by the white horizontal lines. (b) Image showing the tissue column at 64 different *b*-factors from 5 to 6000 s/mm^2 (top-to-bottom). Note the two lipid bands at both the left and right hand sides arising from slowly diffusing fatty acids in the marrow (inner band) and subcutaneous fat in the scalp (outer bands). Note also the prolongation of signal with *b*-factor appearing as centrally located streaks which correspond to the internal capsules

parameters D_1, D_2 and the fraction of the fast ADC component $A_1/(A_1+A_2)$ as functions of position along the brain tissue column. Similar fitting for over 125 brain voxels for each volunteer yielded means and standard deviations for the biexponential parameters, which are compiled in Table 2. The bottom row in the table provides inter-individual means and standard deviations of these parameters using data from all eight volunteers. These parameters from global brain tissue suggest that over a *b*-factor range of 195–6000 s/mm^2, some 74% of the water is associated with a fast diffusion coefficient typical of previously reported values, while 26% is associated with a much slower diffusion coefficient. Regional differences were observed from different brain areas along the column, however. Measurements made from the internal capsule, identified as the central streaks in Fig. 3(b), yielded a significantly lower inter-individual mean volume fraction for the fast ADC component of 0.59 ± 0.09 compared with a value of 0.76 ± 0.07 measured in cortical gray matter ($N = 8$).

Although the signal from methylene and methyl protons of lipid in subcutaneous fat and the scalp showed very little decay with *b*-factor, the extended range of *b*-factors resulted in the measurement of a consistent negative slope from semi-log plots of lipid signal, as seen in Fig. 4. Thus we report an estimate of the lipid diffusion coefficient in the scalp, obtained by pooling the data from all eight volunteers, as 0.053 ± 0.02 μm^2/ms (mean ± SD). This is some 26 times smaller than the fast ADC value obtained for brain water but only five times smaller than the slow ADC value obtained from the second component in the biexponential fits to brain water signal decay (Table 2).

A detailed study of brain signal intensity with increasing *b*-factor over the smaller but clinically more typical *b*-factor range of 5–2000 s/mm^2 was performed in one volunteer in addition to the study made in the 5–6000 s/mm^2 range at the same *TE*, but using all three gradient axes. Constraining the maximum *b* value to 2000 s/mm^2 allowed for the use of only one gradient axis for diffusion sensitization so that individual data sets could be acquired with diffusion sensitization along the *x*, *y* and *z* axes separately. Figure 6 shows brain signal decays with *b*-factor as taken from 0.45 ml voxels in the cortex and in the internal capsule, respectively, with diffusion sensitization along each axis separately. None of these six decay curves display any remarkable curvature in the semi-log plots over this *b*-factor range and so they were fit with monoexponential decay functions, shown as solid lines. Data from the cortex showed minimal sensitivity to the direction of the diffusion sensitizing gradient with an average ADC trace value of 0.75 ± 0.03/ms as taken from the monoexponential fits. Data from the internal capsule showed a pronounced dependence on gradient direction with a rapid decrease of signal with diffusion sensitization along *z*, parallel to the largely inferior-to-superior fiber orientation in the internal capsule. The ADC measured along *z* in the internal capsule was 0.96 μm^2/ms, nearly twice that measured along the *x* and *y* axes where ADC values of 0.43 and 0.51 μm^2/ms were measured, respectively. Figure 7 shows that, when the range of *b*-factors was extended by using all three gradient directions for diffusion sensitization, both decay curves show pronounced non-monoexponential behavior well-characterized by the biexponential fits shown as solid lines. With the biexponential analysis, the fast ADC component for each curve was approximately 1.2 μm^2/ms, substantially higher than that obtained for a single ADC component using *b*-factors less than 2000 s/mm^2.

Figure 8 show 3 mm thick contiguous axial slices through the mid-supratentorial brain region of a healthy volunteer. The three white boxes in the contiguous slices define a homogeneous region of the putamen encompassing approximately $10 \times 10 \times 4$ mm^3. This region was interrogated with the line scan diffusion sequence using 10 mm thick excitation and refocusing pulses and a receiver bandwidth/no. of frequency encoding steps of

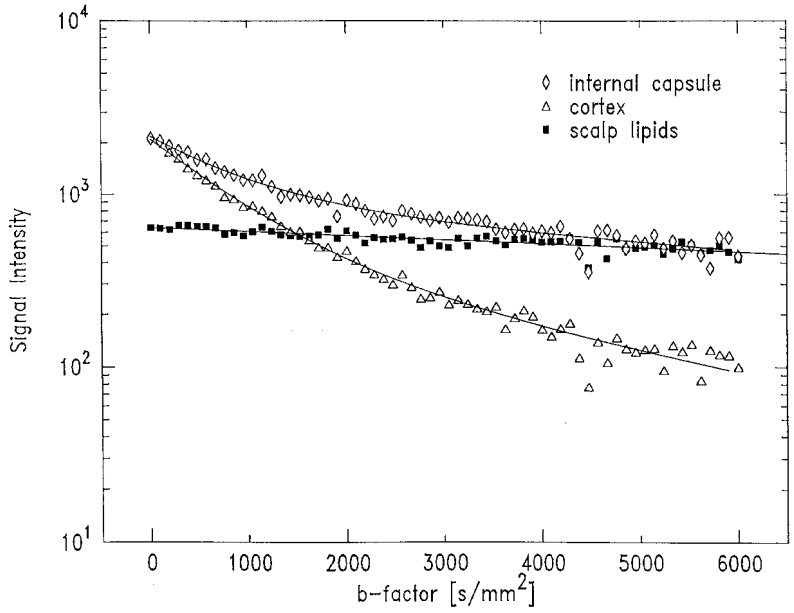

Figure 4. Typical signal decay curves from brain tissue and scalp lipids extracted from data sets such as that shown in Fig. 3(b). The decays from the two brain voxels (internal capsule and cortex) show definite curvature on the semi-log plot and so are clearly non-monoexponential. These decays have been fitted with biexponential functions, as shown by the solid lines through the data. Scalp lipid decay was fit with a monoexponential function (solid line)

8/128 to obtain an along-column resolution of approximately 2 mm. A signal decay curve from the $10 \times 10 \times 4\ mm^3$ voxel in the putamen is shown in Fig. 9 along with the baseline noise profile taken from a region outside of the head. The smooth fit through the experimental curve made with biexponential fitting parameters similar to those reported in Table 2 (figure legend) indicates that partial volume averaging between either gray/white matter or brain/CSF cannot be responsible for the observed non-monoexponential behavior that we have consistently observed in these studies using thicker columns.

DISCUSSION

Routine diffusion imaging of the brain utilizes two or at most a few *b*-factors which are generally restricted to values under 2000 s/mm^2. Brain ADC maps are then generated assuming a monoexponential decay of signal with *b*-factor with values for the ADC parameter in the human brain reported to be of the order of 1 μm^2/ms.[1–10] In order to account for areas in which anisotropic diffusion is present, additional images are often acquired using different directions of the diffusion sensitizing gradient. In this manner "trace" ADC maps and anisotropy maps of varying degrees of complexity, up to and including full diffusion tensor imaging,[12] may be generated.

We refer to the implicit assumption of a monoexponential signal decay of brain water with increasing *b*-factor, coupled with a sensitivity to diffusion gradient direction, as the 'standard' model. Departures from the standard model have been noted by some investigators who utilized detailed measurements in the very small *b*-factor regime below 200 s/mm^2. Such low *b*-factor studies may possibly be used to separate fast 'perfusion' and/or cerebrospinal fluid (CSF) ADC components from the more prominent brain water diffusion component with its smaller ADC.[16–18] The 'perfusion' component generally reported in such studies had ADC values greater than that of pure water at 37°C[8] and was much smaller in amplitude than the primary brain water component. Although some of the very first few points of our data may be affected by such a fast ADC component, the bulk of our measurements were made over a range of *b*-factors in which the effects of a small water fraction with a high ADC should be negligible.

In the work of Niendorf *et al.* with *in vivo* rat brain, biexponential brain signal decay over the *b*-factor range of 10–10 000 s/mm^2 at a fixed *TE* of 54 ms was observed.[19] Using a single voxel PRESS technique with a *TE* of 54 ms, they reported a fraction for the fast ADC component of the order of 0.8 and ADC values for the fast and slow components of approximately 0.8 and 0.2 μm^2/ms, respectively. This rat brain data is consistent with our findings in humans, where we have used a longer echo time of 175 ms and a more limited *b*-factor range up to

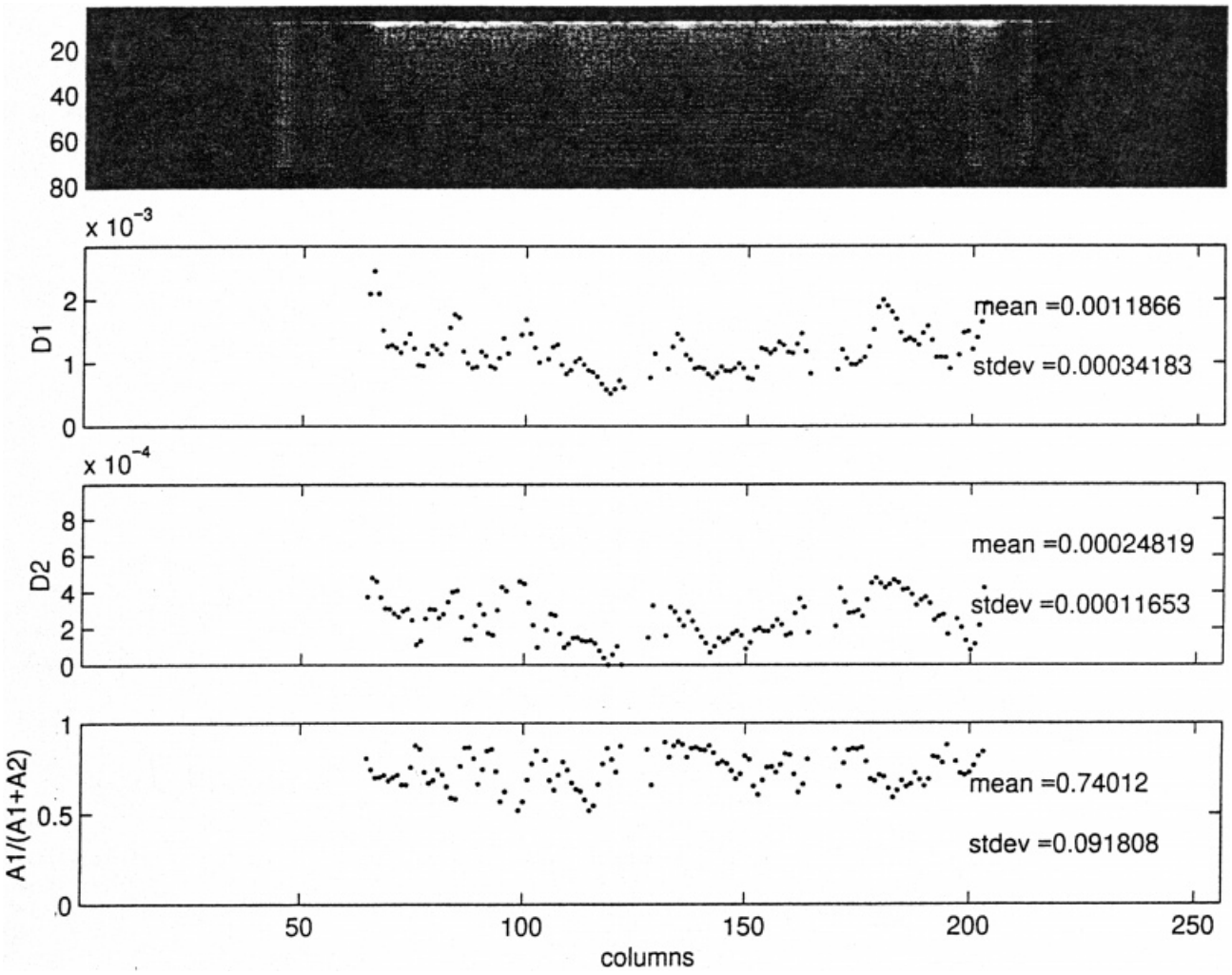

Figure 5. Automated fitting of brain voxel signal decays with *b*-factor to biexponetial functions. Shown is the original data (top) and the biexponential parameters D_1, D_2, and the fraction $A_1/(A_1 + A_2)$ for each $15 \times 15 \times 1$ mm^3 voxel in the brain. The means and standard deviations for all brain voxels are shown in each case with the two diffusion coefficients reported in units of mm^2/s

only 6000 s/mm^2. Any experimental or systematic errors which might lead to non-monoexponential signal behavior, possibly from imaging/diffusion gradient cross-terms or eddy current sources, have been precluded in either study on the basis of the well-behaved mono-exponential decays observed in various isotropic solutions (Figs 1 and 2). With the spatial localization capabilities of the line scan method, we have also demonstrated that the biexponential behavior is not restricted to brain tissue in which anisotropic ADC behavior is obvious, as in the internal capsule. Rather, this type of decay is typical of all the brain voxels studied, including regions of the cortex where minimal anisotropy is observed (Fig. 6). Partial volume averaging between different brain tissues also seems an unlikely candidate for the explanation of biexponential behavior, as the results from Figs 8 and 9 demonstrate.

Table 2. Intra-individual means and standard deviations (SD) of biexponential parameters D_1, D_2, and the fast ADC fraction $A_1/(A_1 + A_2)$. This data was evaluated for each of the eight individuals using more than 125 brain voxels per study, as shown in Fig. 5. The inter-individual means ± SD are provided in the bottom row

Subject	D_1 (μm^2/ms)	D_2 (μm^2/ms)	$A_1/(A_1 + A_2)$
1	1.34 ± 0.22	0.24 ± 0.09	0.74 ± 0.10
2	1.19 ± 0.34	0.25 ± 0.12	0.74 ± 0.09
3	1.31 ± 0.36	0.20 ± 0.11	0.77 ± 0.10
4	1.22 ± 0.60	0.25 ± 0.12	0.72 ± 0.13
5	1.42 ± 0.83	0.24 ± 0.15	0.73 ± 0.12
6	1.40 ± 0.48	0.27 ± 0.15	0.74 ± 0.10
7	2.02 ± 1.18	0.25 ± 0.09	0.75 ± 0.13
8	1.32 ± 0.36	0.28 ± 0.10	0.73 ± 0.09
Mean ± SD	1.40 ± 0.26	0.25 ± 0.03	0.74 ± 0.02

One possibility for two ADC components is water compartmentation between intra- and extracellular water pools. In this case it is reasonable to assume that water molecules within the cells would be associated with the component having the smaller ADC value as a consequence of interactions with intracellular organelles and

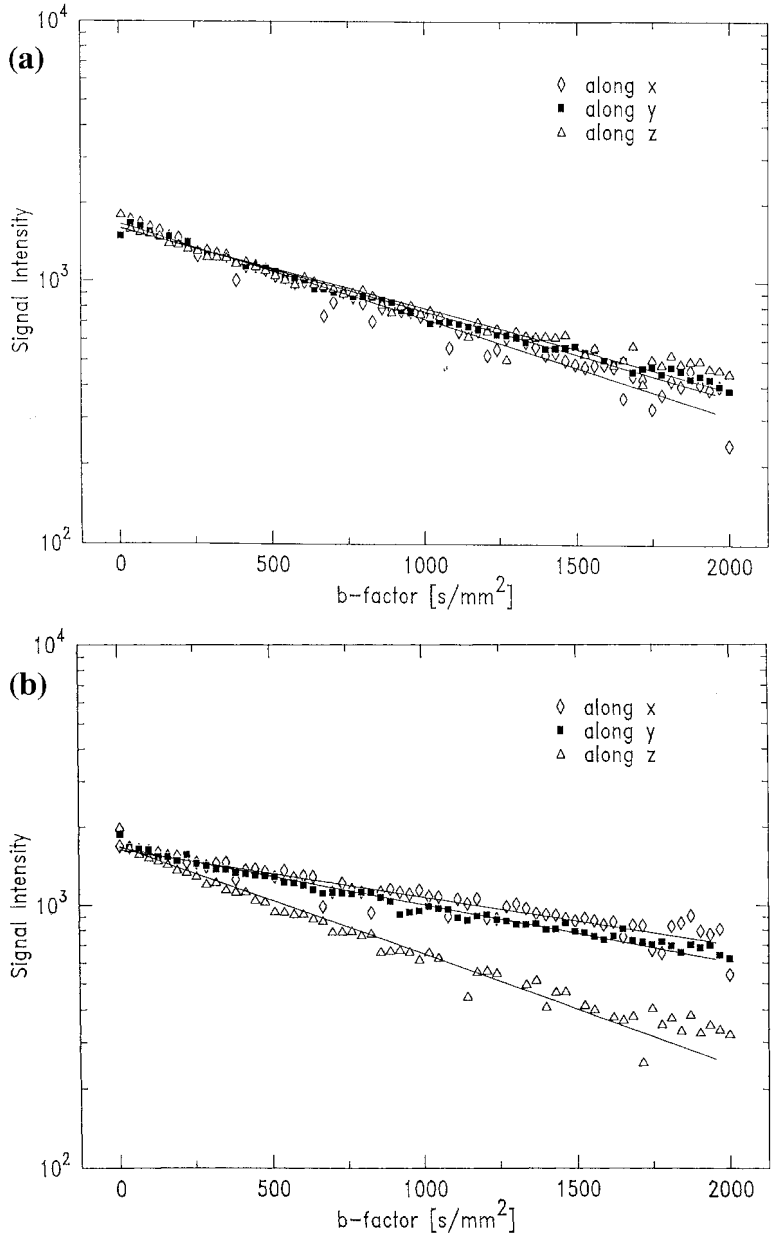

Figure 6. (a) Brain signal decay with *b*-factor from a voxel in the cortex acquired over the more limited *b*-factor range from 5 to 2000 s/mm^2 but with diffusion sensitization along each spatial axis *x, y* and *z*, separately. Any curvature is difficult to detect over this range and the decays have been fitted with monoexponential functions (solid lines) with slopes showing no marked dependence on the direction of the diffusion sensitization gradients. (b) Brain signal decay with *b*-factor from a voxel in the internal capsule acquired over the more limited *b*-factor range from 5 to 2000 s/mm^2 but with diffusion sensitization along each spatial axes *x, y* and *z*, separately. Although any curvature is difficult to detect over this range and the decays have been fitted with monoexponential functions (solid lines), the slopes do show a marked dependence on the direction of the diffusion sensitization gradients, indicating anisotropic diffusion processes

membranes. Although difficult to quantify analytically, diffusive motions which are restricted to cellular dimensions cause significant decreases in measured diffusion coefficients. As an example, using the analytic expression for one-dimensional diffusion between impermeable barriers discussed by Stanisz *et al.*,[26] we calculate that a barrier separation of 10 μm would result in a free diffusion coefficient of 1.5 μm^2/ms to appear to have an

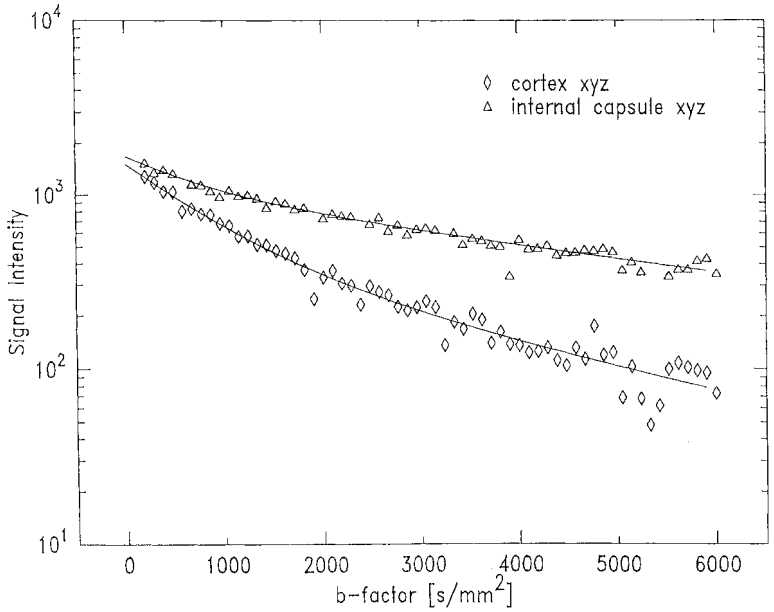

Figure 7. Shown are the brain signal decays over the full *b*-factor range of 5–6000 s/mm^2 for the same two brain voxels used for Fig. 6, but using all three gradients simultaneously (*xyz*) to obtain the largest *b*-factors. Note the decided curvature of the brain signal decays which have been fitted with biexponential functions (solid lines). The data in this figure and Fig. 6 indicate that the biexponential behavior does not depend on anisotropic diffusion

extremely small diffusion coefficient of only 0.06 μm^2/ms under our measurement conditions. Thus, low apparent diffusion coefficients similar to that extracted for the second ADC component of our analyses are not unreasonably expected for intracellular water. Indeed, values in the 0.2–0.5 μm^2/ms range for intracellular diffusion coefficients have been measured from cell culture preparations.[27] It is tempting therefore, to associate the high ADC component of our measurement with an extracellular water population and the small ADC component with an intracellular water population. A problem then arises in interpreting the relative volume fractions of these components. In typical brain voxels located well outside ventricular spaces, the intracellular water volume fraction is known to exceed the extracellular and/or interstitial water volume fraction. From our data and that of Niendorf *et al.*,[19] however, it is the component with the highest ADC value which also has the highest volume fraction. This makes the interpretation of intra- vs extracellular water compartmentation somewhat problematic, even if one considers the possibility of water exchange between compartments, a subject we now discuss in greater detail.

Karger *et al.*[28] developed an expression for the signal decay with *b*-factor from a system consisting of two compartments with different intrinsic diffusion coefficients but which are in exchange with one another. The solution for the decay is biexponential in form, like eq. (4). However, the apparent diffusion coefficients D_1 and D_2, and the apparent volume fractions A_1 and A_2, change with *b*-factor. In particular, for a normalized decay in which $A_1 + A_2 = 1$ and for which we define $D_1 > D_2$, these parameters read

$$D_{1,2} = [D_f + D_g + (k_{fg} + k_{gf})/(\gamma\delta G)^2]/2 \pm \Psi \qquad (5)$$

where

$$2\Psi = \{[D_f - D_g + (k_{fg} - k_{gf})/(\gamma\delta G)^2]^2 + 4k_{fg}k_{gf}/(\gamma\delta G)^4\}^{1/2} \qquad (6)$$

and

$$A_2 = (gD_g + fD_f - D_1)/(D_2 - D_1) \qquad (7)$$

Here, f and g are the actual volume fractions of the two pools with $f + g = 1$, k_{fg} and k_{gf} are the exchange rates in 1/s between the fractions which are constrained by the steady-state relationship $fk_{fg} = gk_{gf}$. D_f and D_g are the intrinsic diffusion coefficients within each compartment. Only in the absence of exchange will the parameters extracted experimentally from biexponential fits of signal intensity vs *b*-factor directly reflect the intrinsic volume fractions and diffusion coefficients of each compartment. In the more general case of exchange these parameters depend on the *b*-factor through the gradient strength G and the timing variables δ and Δ.

Based on the above formalism, simulations of the signal decay with *b*-factor were generated for the same

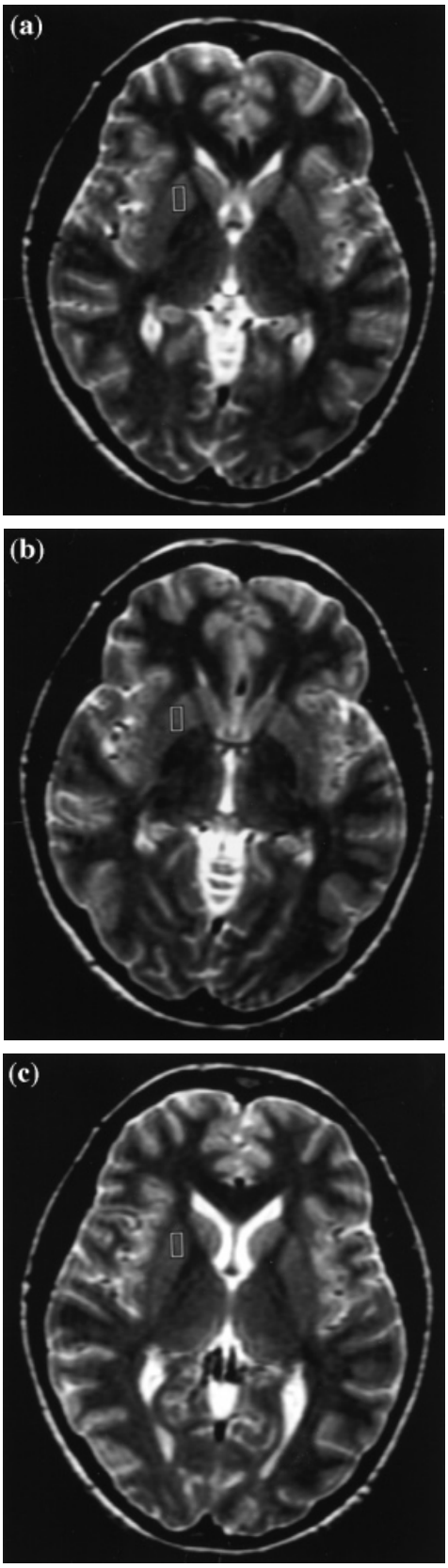

Figure 8. Contiguous axial 3 mm thick T_2-weighted fast spin-echo images (*TR*/*TE*/*ETL* = 2000/85/8) of the brain of a healthy volunteer in which a box outlines the region in the putamen ($10 \times 10 \times 4$ mm^2 voxel size) from which the diffusion decay curve in Fig. 9 was extracted

conditions used in our experiments. Figure 10 shows three such curves, all of which would be difficult to distinguish experimentally from our data and from each other given the typical signal variations shown in Fig. 4. The simulated curves of Fig. 10 arise, however, from three quite different conditions of the two-site exchange diffusion model. The curve depicted by the circles was generated assuming no exchange between compartments ($k_{fg} = 0$) and with the diffusion coefficients and fractional amplitudes taken from the bottom row in Table 1 with $g = 0.74$, $D_g = 1.4\ \mu m^2/ms$ and $D_f = 0.25\ \mu m^2/ms$. As mentioned above, this is largely opposite to the volume fraction/ADC value relationship expected if an interpretation based on intra- vs extracellular water compartmentation in brain tissue is to be made. It is possible, however, that the intracellular pool is more heavily T_2-weighted than the extracellular pool at the long *TE* of 175 ms, thereby appearing as a much smaller fraction. One can reverse the order of the volume fractions, setting $f = 0.74$, and keep D_f as the lower ADC value of $0.25\ \mu m^2/ms$, turn on an exchange rate from the *f* pool to the *g* pool of 10/s and obtain the curve represented by the stars in Fig. 10. As may be seen there is only a subtle difference between this curve (stars) and that obtained for the case of no exchange (circles) and so this curve too would nicely characterize the data. However, in order to make the latter curve acceptable, the larger of the two ADC values was raised to $4.4\ \mu m^2/ms$, approximately 1.5 times the diffusion coefficient of pure water at 37°C.[8] The exchange rate of 10/s corresponds to an average intracellular water molecule lifetime of 100 ms and seems quite reasonable based on red cell water permeability studies.[29,30] However, within the confines of a simple two-site exchange diffusion model, forcing the volume fractions, rank order of ADC values, and exchange rates to fit with an intra- vs extracellular interpretation resulted in an unacceptably large value for the extracellular diffusion coefficient. The third curve in Fig. 10 (crosses) was generated by keeping the volume fractions at 0.74 and 0.26 for the fast and slow ADC components, *g* and *f*, respectively. The fast ADC value was left at $1.4\ \mu m^2/ms$, as obtained from the biexponential fits, but the slower ADC value was lowered to a value of $0.07\ \mu m^2/ms$ and the exchange rate was left as $k_{fg} = 10/s$. This model, also quite acceptable from a data characterization standard, implies a pool with a very slow diffusion coefficient in exchange with a larger pool having a fast diffusion coefficient. An interpretation of 'free' vs 'bound' water seems tenable for this particular set of exchange parameters, as discussed in greater detail by Assaf and Cohen who utilized ^{2}H NMR based diffusion measurements to detect different water populations in excised brain tissue.[31]

Although we have offered several possible interpretations for our findings of non-monoexponential signal behavior with increasing *b*-factor from brain tissue, it is apparent that further modeling and experimentation will

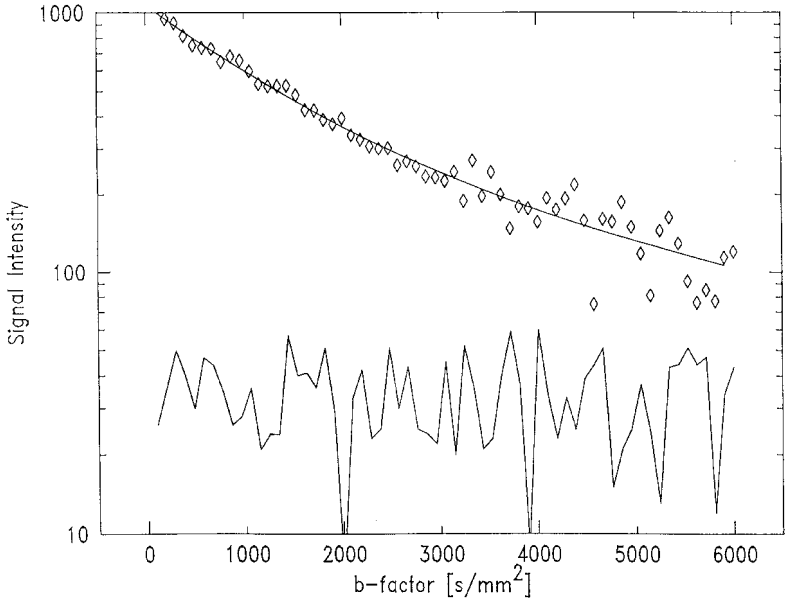

Figure 9. Signal decay with *b*-factor extracted from the voxel indicated in Fig. 8 encompassing pure putamen tissue. Also shown is the baseline noise measurement from the same scan and a solid line fit to the data with a biexponential function with parameters similar to those reported in Table 1 [$D_1 = 0.79\ \mu m^2/ms$, $D_2 = 0.19\ \mu m^2/ms$, $A_1/(A_1 + A_2) = 0.72$]

be required before conclusive interpretations become possible. Effects of exchange, restricted diffusion, anisotropy and intrinsic compartmental diffusion coefficients undoubtedly all play roles in the signal decay over extended *b*-factor ranges, like those used in this study. More complicated models which incorporate these

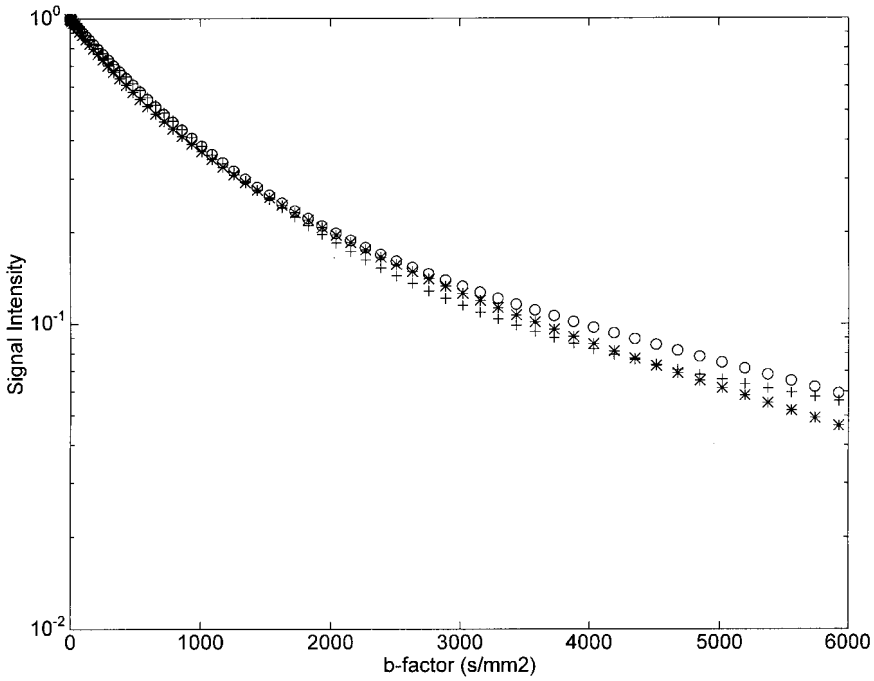

Figure 10. Simulated signal decay curves with *b*-factor generated under conditions mimicking our *in vivo* experiments on the clinical scanner. The three decay curves shown are for three different sets of possible parameters of the two-site exchange diffusion model (see text for details), but would all accommodate the data within the available signal-to-noise levels

effects, like that introduced by Stanisz *et al.* in modeling diffusion behavior in excised optic nerve,[26] should be considered. In the brain, relatively specific increases in extracellular water (e.g. hyponatremia) or intracellular water (e.g. ischemia) may provide direct tests of proposed modeling schemes.

Equally important to any biophysical interpretations of our data, however, is the increased empirical characterization of tissue water diffusion afforded by performing multiple *b*-factor measurements over an extended *b*-factor range. Biexponential characterization of the resulting signal decay appears to be quite robust, as shown above. The line scan format is well suited to performing such measurements in reasonable scan times and may readily be extended to cover greater volumes with no increase in scan time using non-orthogonal slice selective RF pulses.[9,10] The manner in which the biexponential parameters measured over the extended *b*-factor range respond to pathologies such as stroke, tumor or white matter diseases may offer unique insights for diagnosis and monitoring therapy.

REFERENCES

1. Le Bihan, D., Breton, E., Lallemand, D., Grenier, P., Cabanis, E. and Laval-Jeantet, M. MR imaging of intravoxel incoherent motion: application to diffusion and perfusion in neurologic disorders, *Radiology* **161**, 401–407 (1986).
2. Moseley, M. E., Kucharczyk, J., Mintorovitch, J., Cohen, Y., Kurhanewicz, J., Derugin, N., Asgari, H. and Norman, D. Diffusion-weighted MR imaging of acute stroke: correlation with T2-weighted and magnetic susceptibility-enhanced MR imaging in cats. *AJNR* **11**, 423–432 (1990).
3. Moseley, M. E., Cohen, Y., Kucharczyk, J., Asgari, H. S., Wendland, M. F., Tsuruda, J. and Norman, D. Diffusion-weighted MR imaging of anisotropic water diffusion in cat central nervous system, *Radiology* **176**, 439–445 (1990).
4. van Gelderen, P., de Vleeschouwer, M. H. M., DesPres, D., Pekar, J., van Zijl, P. C. M. and Moonen, C. T. W. Water diffusion and acute stroke, *Magn. Reson. Med.* **31**, 154–163 (1994).
5. Warach, S., Gaa, J., Siewert, B., Wielopolski, P. and Edelman, R. R. Acute human stroke studied by whole brain echo planar diffusion-weighted magnetic resonance imaging. *Ann. Neurol.* **37**, 231–242 (1995).
6. Yongbi, M. N., Huang, N. C., Branch, C. A. and Helpern, J. A. The application of diffusion-weighted line-scanning for the rapid assessment of water ADC changes in stroke at high magnetic fields. *NMR Biomed.* **10**, 79–86 (1997).
7. Moonen, C. T. W., Pekar, J., de Vleeschouwer, M. H. M., van Gelderen, P., van Zijl, P. C. M. and Despres, D. Restricted and anisotropic displacement of water in healthy cat brain and in stroke studied by NMR diffusion imaging, *Magn. Reson. Med.* **19**, 327–332 (1991).
8. van der Toorn, A., Sykova, E., Dijkhuizen, R. M., Vorisek, I., Vargova, L., Skobisova, E., van Lookeren Campagne, M., Reese, T. and Nicolay, K. Dynamic changes in water ADC, energy metabolism, extracellular space volume, and tortuosity in neonatal rat brain during global ischemia, *Magn. Reson. Med.* **36**, 52–60 (1996).
9. Gudbjartsson, H., Maier, S. E., Mulkern, R. V., Morocz, I. A., Patz, S. and Jolesz, F. A. Line scan diffusion imaging. *Magn. Reson. Med.* **36**, 509–519 (1996).
10. Maier, S. E., Gudbjartsson, H., Patz, S., Hsu, L., Lovblad, K.-O., Edelman, R. R., Warach, S. and Jolesz, F. A. Line scan diffusion imaging: characterization in healthy subjects and stroke patients. *AJR* **171**, 85–93 (1998).
11. Henkelman, R. M., Stanisz, G. J., Kim, J. K. and Bronskill, M. J. Anisotropy of NMR properties of tissues, *Magn. Reson. Med.* **32**, 592–601 (1994).
12. Pierpaoli, C. and Basser, P. J. Toward a quantitative assessment of diffusion anisotropy, *Magn. Reson. Med.* **36**, 893–906 (1996).
13. Basser, P. J., Mattiello, J. and LeBihan, D. MR diffusion tensor spectroscopy and imaging, *Biophys. J.* **66**, 259–267 (1994).
14. Hajnal, J. V., Doran, M., Hall, A. S., Collins, A. G., Oatridge, A., Pennock, J. M., Young, I. R. and Bydder, G. M. MR imaging of anisotropically restricted diffusion of water in the nervous system: technical, anatomic, and pathologic considerations, *J. Comput. Assist. Tomogr.* **15**, 1–18 (1991).
15. Pierpaoli, C., Jezzard, P., Basser, P. J., Barnett, A. and Di Chiro, G. Diffusion tensor imaging of the human brain, *Radiology* **201**, 637–648 (1996).
16. Le Bihan, D., Breton, E., Lallemand, D., Aubin, M. L., Vignaud, J. and Laval-Jeantet, M. Separation of diffusion and perfusion in intravoxel incoherent motion MR imaging. *Radiology* **177**, 401–405 (1990).
17. Le Bihan, D., Moonen, C. T. W., van Zijl, P. C. M., Pekar, J. and DesPres, D. Measuring random microscopic motion of water in tissues with MR imaging: A cat brain study, *J. Comput. Assist. Tomogr.* **15**, 19–25 (1991).
18. Morvan, D. In vivo measurement of diffusion and pseudo-diffusion in skeletal muscle at rest and after exercise. *Magn. Reson. Imag.* **13**, 193–199 (1995).
19. Niendorf, T., Dijkhuizen, R. M., Norris, D. G., van Lookeren Campagne, M. and Nicolay, K. Biexponential diffusion attenuation in various states of brain tissue: implications for diffusion-weighted imaging. *Magn. Reson. Med.* **36**, 847–857 (1996).
20. Oshio, K. and Mulkern, R. V. Rapid fat/water assessment in knee cavity bone marrow by inner volume spectroscopic imaging with RARE. *J. Magn. Reson. Imag.* **2**, 601–604 (1992).
21. Chenevert, T. L., Brunberg, J. A. and Pipe, J. G. Anisotropic diffusion in human white matter: demonstration with MR techniques *in vivo*. *Radiology* **177**, 401–405 (1990).
22. Siegel, C. L., Aisen, A. M., Ellis, J. H., Londy, F. and Chenevert, T. L. Feasibility of MR diffusion studies in the kidney, *J. Magn. Reson. Imag.* **5**, 617–620 (1995).
23. Stejskal, E. O. and Tanner, J. E. Spin diffusion measurements: spin echoes in the presence of a time-dependent field gradient. *J. Chem. Phys.* **42**, 288–292 (1965).
24. Mulkern, R. V., Wong, S. T. S., Jakab, P., Bleier, A. R., Sandor, T. and Jolesz, F. A. CPMG imaging sequences for high field *in vivo* transverse relaxation studies. *Magn. Reson. Med.* **16**, 67–79 (1990).
25. Wood, M. L., Bronskill, M. J., Mulkern, R. V. and Santyr, G. E., *J. Magn. Reson. Imag.* **3**(suppl.), 19–26 (1993).
26. Stanisz, G. J., Szafer, A., Wright, G. A. and Henkelman, R. M. An analytical model of restricted diffusion in bovine optic nerve. *Magn. Reson. Med.* **37**, 103–111 (1997).
27. Pilatus, U., Shim, H., Artemov, D., Davis, D., van Zijl, P. C. M. and Glickson, J. D. Intracellular volume and apparent diffusion constants of perfused cancer cell cultures, as measured by NMR, *Magn. Reson. Med.* **37**, 825–832 (1997).
28. Karger, J., Pfeifer, H. and Heink, W. Principles and applications of self-diffusion measurements by NMR, *Adv. Magn. Reson.* **12**, 1–89 (1988).
29. Herbst, M. D. and Goldstein, J. H. A review of water diffusion measurement by NMR in human red blood cells, *Am. J. Physiol.* **256**, C1097–C1104 (1989).
30. Mulkern, R. V., Bowers, J. L., Guttmann, C. R. G. and Sadowski, R. High field proton spin-lattice relaxation studies of water exchange parameters in red cell suspensions, *Phys. Med. Biol.* **41**, 255–268 (1996).
31. Assaf, Y. and Cohen, Y. Detection of different water populations in brain tissue using ^{2}H single- and double-quantum-filtered diffusion NMR spectroscopy, *J. Magn. Reson. Ser. B* **112**, 151–159 (1996).

